Table 1. Excess partial molar thermodynamic quantities of solution for oxygen as a function of temperature. These represent the change of the total thermodynamic quantity resulting from the transfer of one mole of oxygen from a hypothetical solution, in which there is one mole of oxygen per liter, to a hypothetical molar solution of sea water of unit chlorinity. Unit Cl: unit chlorinity, sea salt.

Temperature (°C)	Cal (mole O_2)$^{-1}$ (unit Cl)$^{-1}$		Cal deg^{-1}(mole O_2)$^{-1}$ (unit Cl)$^{-1}$	
	$\Delta\tilde{G}_{O_2}^{xs}$	$\Delta\tilde{H}_{O_2}^{xs}$	$\Delta\tilde{S}_{O_2}^{xs}$	$\Delta\tilde{C}p_{O_2}^{xs}$
0	6.92	24.3	0.064	(−0.7)
10	6.43	17.3	.038	(−0.7)
20	6.14	10.0	.013	(−0.7)
30	6.12	2.5	−0.012	(−0.8)

coefficient of the gas; in fact, the former may be avoided completely in thermodynamics by use of the latter.

$$\Delta\tilde{G}_{O_2}^{xs} = -RT \log \beta \qquad (3)$$

Substituting the experimental relation of Eq. 1 in Eq. 3, we obtain

$$\Delta\tilde{G}_{O_2}^{xs} = RT\ k(t)\ \mathrm{Cl} \qquad (4)$$

The determined excess partial molar free energy, as calculated from the experimental data by use of Eq. 4, was fitted to a temperature curve to yield smooth first and second derivatives:

$$k = -0.1288 + \frac{53.44}{T} - 0.04442 \log_e T + 7.145 \cdot 10^{-4}\,T \qquad (5)$$

where T is the absolute temperature and k is given in reciprocal parts per thousand. From this smooth function the excess partial molar thermodynamic quantities were computed on a unit-chlorinity basis (Table 1). The root-mean-square (standard) deviation of the calculated excess free energy is within about 3 percent over a range of 35°C, or about 12 percent of the absolute temperature. The accuracy of the excess enthalpy and of the excess entropy, obtained from the temperature derivative, is of the order of 25 percent. Further differentiation to obtain the excess heat capacity cannot yield accurate values, but the calculated excess heat capacities are shown in parentheses in Table 1 to indicate merely that they are small negative quantities.

It is noted that the large exothermic (negative) heat of aqueous solution of oxygen (characteristic of N_2, Ar, and the other inert gases) is reduced significantly by the addition of even small amounts of sea salt. (Unit-chlorinity sea water is equal in ionic strength to a $0.037M$ solution of 1 : 1 electrolyte.) Frank and Evans (*11*) have suggested that the observed entropies of solution and the enormous positive partial molar heat capacities of solution for the inert gases are consistent with a model picturing the solute gas as producing a more highly structured order of the water molecules in its vicinity. The data of Table 1 suggest that addition of sea salt (mainly NaCl) results in disorganization of this induced structure.

E. J. GREEN*
D. E. CARRITT

Department of Geology and Geophysics, Massachusetts Institute of Technology, Cambridge

References and Notes

1. C. J. J. Fox, *Conseil Perm. Intern. Exploration Mer Publ. Circonstance* **41** (1907); G. A. Truesdale *et al.*, *J. Appl. Chem. London* **5**, 53 (1955).
2. For details of the measurements see E. J. Green, "A redetermination of the solubility of oxygen in sea water and some thermodynamic implications of the solubility relations," thesis, Dept. of Geology and Geophysics, Massachusetts Institute of Technology, 1965.
3. J. H. Carpenter, *Limnol. Oceanog.* **10**, 135 (1965).
4. A. B. Arons and C. F. Kientzler, *Trans. Amer. Geophys. Union* **35**, 722 (1954).
5. By cooperation with Woods Hole Oceanographic Institution. Oceanographers generally employ the concentration unit chlorinity that we have used; it was the parameter most directly measured. Ionic strength is of more physical-chemical interest; it has been shown [J. Lyman and R. H. Fleming, *J. Marine Res. Sears Found. Marine Res.* **3**, 134 (1940)] to be related to the chlorinity by

$$I = 0.00147 + 0.03592\ \mathrm{Cl} + 0.000068\ \mathrm{Cl}^2$$

6. R. G. Paquette, *NAS–NRC Publ. 600* (1959), pp. 128–45.
7. J. Setschenow, *Mem. Acad. Imp. Sci. St. Petersburg* **22**(6) (1875); *Z. Physik. Chem.* **4**, 117 (1889).
8. J. H. Carpenter, *Limnol. Oceanog.* **11**, 264 (1966).
9. W. F. McDevit and F. A. Long, *J. Amer. Chem. Soc.* **74**, 1773 (1952); *Chem. Rev.* **51**, 119 (1952).
10. M. Randall and C. F. Failey, *Chem. Rev.* **4**, 271 (1927).
11. H. S. Frank and M. W. Evans, *J. Chem. Phys.* **13**, 507 (1945).
12. Research sponsored by NSF grants GP-486 and GA-702.
* Present address: Carnegie Institute of Technology, Pittsburgh, Pa. 15213.

24 April 1967

Bistatic-Radar Detection of Lunar Scattering Centers with Lunar Orbiter I

Abstract. *Continuous-wave signals transmitted from Lunar Orbiter I have been received on Earth after they have been reflected from the surface of the moon. The frequency spectrum of the reflected signals is used to locate discrete, heterogeneous, scattering centers on the lunar surface. The scattering centers are probably distinguished from the surrounding terrain by a higher surface reflectivity. Continuous-wave bistatic radar could provide an important new method for the study and mapping of planetary surfaces.*

The dispatch of space probes to the moon and planets has made it possible to study the surfaces of these objects with bistatic radar, that is radar with well-separated transmitter and receiver, one on Earth and the other carried into space on the probe. We here discuss a case where transmissions originated on the spacecraft, were reflected from the surface of the moon, and finally received on Earth. The opposite, or up-link, case is analytically equivalent and may be preferred for planetary studies because of the much greater power available from Earth-based transmitters.

We here present a preliminary analysis of the first bistatic-radar echoes obtained from a celestial body in order to (i) provide initial bistatic-radar evidence of the heterogeneity of the lunar surface, (ii) demonstrate the fact that the echo spectrum for continuous-wave illumination carries information from which a two-dimensional, radar-reflectivity map of the lunar surface can be constructed, and (iii) illustrate the potential of bistatic radar for eventual detailed mapping and radar-reflectivity studies of planetary surfaces.

The measurements described here were made on 12 October 1966, with the Lunar Orbiter I spacecraft. For the purposes of this experiment, the radiation from the spacecraft, which was emitted through an omnidirectional antenna, consisted essentially of a 100-milliwatt carrier at 2295 Mhz. The signal received on the ground consisted of this carrier and an image of the carrier reflected in the moon. Since the length of the direct path from the ground to the spacecraft varies at a different rate than does the length of the path followed by the reflected energy, the two signals (the direct and reflected) undergo different Doppler shifts and may be distinguished by their relative positions in the frequency spectrum. In addition, the reflected signals suffer spectral broadening and loss of strength. The Doppler shift of the direct signal was extracted by the receiving system on the ground so that reflected signals could be measured relative to the carrier in both amplitude and frequency.

The radar parameters were: radiated carrier power, 100 milliwatts continuous wave; antenna gain (transmitting), −1 db; antenna gain (receiving), +57 db; system temperature during data pass, ~80°K.

At the time this record was made (Fig. 1), the spacecraft, which was in a near-equatorial orbit over the Crater Kastner and Mare Smythii on the moon's eastern limb, was approaching its minimum altitude of about 40 km. The spacecraft moved around the eastern limb a few degrees below the lunar equator and disappeared at the time indicated as "occultation immersion" on the record.

Because of their continuity, the bright traces on the record are presumed to result from discrete areas, or scatterers, on the lunar surface. Since the Doppler shift of the direct signal—which is used as a reference frequency—changes slowly compared with the Doppler shift of the reflected signal, the traces may be visualized as the last portion of the S-shaped time-frequency curve produced by a transmitter moving past a stationary point. Figure 2 presents the data of Fig. 1 graphically.

It is possible to locate the scattering areas on the lunar surface (Fig. 3) by a simple technique. The quantity given on the record is

$$\Delta f = \Delta f_R - \Delta f_D \qquad (1)$$

where Δf_R *is* the Doppler shift of the signal from the scattering area and Δf_D is the Doppler shift of the signal directly from the spacecraft. The Doppler shift of the reflected signal, Δf_R, can be determined since Δf is measured from the record and Δf_D may be calculated from the known orbit of the spacecraft. Furthermore, Δf_R is related to the spacecraft velocity vector by

$$\Delta f_R = \frac{\mathbf{v}}{\lambda} \sin \theta \qquad (2)$$

where θ is the angle between the spacecraft velocity vector and the direction vector to the lunar scattering point, and $\mathbf{v}$ is the velocity of the spacecraft. The motion of the moon gives only a negligible contribution. Thus a measurement of Δf_R defines a cone, with included half-angle θ, about the velocity vector. The intersection of this cone with the surface of the moon defines a locus on the surface in which the scatterer must lie. By determining Δf_R at different times, several loci are generated and a point scatterer must lie at their intersection. There is a twofold ambiguity which results from symmetrical intersections on either side of the spacecraft's ground track on the moon. However, when the possible locations are compared with the instantaneous point of specular reflection, one group of targets, those south of the ground track, consistently correspond to forward scattering and fall on or near

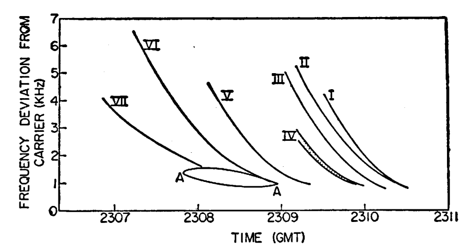

Fig. 2. A simplified drawing of the record in Fig. 1. The traces are identified by roman numerals. The oval region is distinguished from the traces by the letter A.

the specular point. Consequently, these near-specular locations, which would be expected to represent the stronger scattering, were chosen as the positions of the scattering areas in preference to the alternate points which correspond to oblique scattering.

A similar procedure was followed in the case of region A, though in this case several points were simply picked from around the border of the region.

Trace III is a special case. The loci intersected in two areas, which have been designated IIIa and IIIb. The area which contributed to the beginning of the trace is different from that at the end. The transition between the two is apparently continuous. Of a total of 36 intersections, 10 were at IIIa and 15 were at IIIb, with 11 intersections falling at intermediate locations. As indicated by the size of the squares in Fig. 3, the points at a and b were very closely packed. Some of the other areas, notably VI, also show some apparent motion of the target. However, only in the case of trace III could we be certain that this effect is real.

In general, the spacecraft is moving away from the scatterer and into the region of specular reflection, while the signal strength from the scatterer remains constant. Since the signal strength from an isotropic scatterer would fall off as the inverse square of the range, we can only conclude that the strength of the scattering increases sharply in the specular direction given by the mean lunar surface. The angular half-power width of the scattered lobe appears to be on the order of 0.1 radians.

Enhanced scattering must come from distinct variations in the general shape of the surface, the surface reflectivity, or some combination of the two. We conclude that the scatterers can only be accounted for by an enhanced reflectivity in the scattering centers, possibly coupled with local variations in surface roughness, slopes, or shadowing.

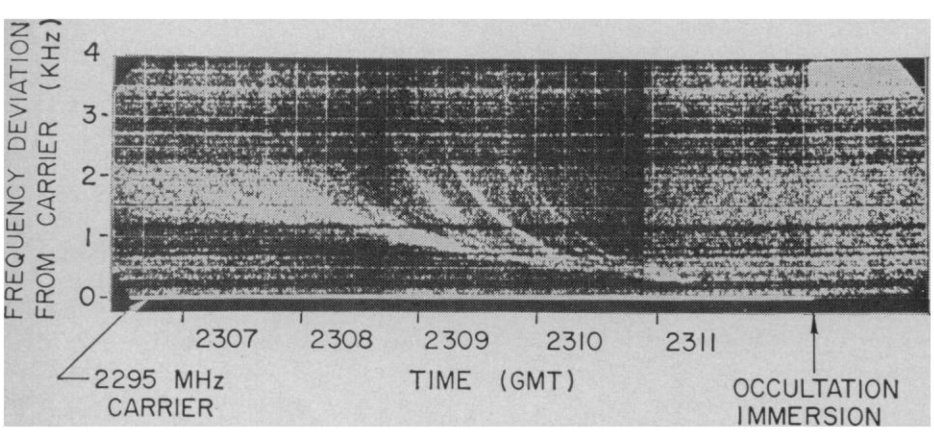

Fig. 1. Time–frequency variations of reflected signals. Time advances to the right; frequency, measured from the carrier, is the ordinate. Signal intensity is represented by the relative brightness of the various portions of the figure. The speckled background is noise, while the constant horizontal lines are spurious responses due to imperfect filtering.

The salient feature of the scattering is the intermittent occurrence of strong, relatively narrow lobes from discrete areas. A model based on changes in reflectivity from place to place can explain these observations. An alternate explanation might be that the signals are the result of reflections from large, relatively smooth undulations in the surface, such as occurs in the reflection of sunlight from the top of a wave. Such a mechanism might be provided by the side of a mountain or the rim of a crater. If the surface were uniformly reflective, then an individual reflection point in such a model would be expected to show some motion along a path more or less parallel to the specular track, and this does not occur. At the same time, the angular width of the scattered lobes in space clearly indicates either that the slopes vary within the scattering center, or that the scatterers are rough, or possibly both.

We should also consider whether or not variations in small-scale roughness alone can provide a satisfactory model. Unless the scatterers correspond to relatively smooth areas of the surface, small-scale roughness would be expected to attenuate rather than to enhance the signal in a given direction, since the roughness would result in a more uniform distribution of the scattered energy in the space above the surface. However, this would require a moon which is extremely rough on the average, in contradiction to the conclusions of Earth-based, monostatic-radar observations. Thus, while this possibility cannot be entirely ruled out on the basis of the results given here, it seems unlikely.

Shadowing is the third effect which must be taken into account. Clearly, this will play an increasingly important role as the orbiter approaches occultations. It is a simple matter to visualize the last several scatterers as standing out in the spectra because they are the only objects near the limb which are high enough to be illuminated. Still, this does not invalidate the arguments already given, particularly near the beginning of the record. In addition, other records taken near the center of the lunar disk where shadowing would not be present exhibit the characteristics which we have associated with the discrete scatterers. However, shadowing may have the effect of hiding some scattering centers for the region shown in Fig. 3. Estimates based on optical photographs of the terminator indicate that shadowing is important within 5° of the limb.

Thus we are unable to give a satisfactory explanation for the observations by slopes, roughness, or shadowing if these three mechanisms are taken independently; nor does it seem probable that some combination of these would be satisfactory. However, we cannot be certain that this is not the case. On the other hand, the addition of variations in surface reflectivity does provide a model which will explain the observations, and this appears to be the most probable explanation. If correct, this conclusion requires that the material in the scattering areas be considerably more compact, or markedly depart in some other way, from the material in the surrounding areas. The traces are generally 3 to 4 db above the level of the noise with III being the strongest trace at 5.5 db above the system noise. Thus, we can say that the enhancement factor has a value of at least 3 and may be considerably larger. Similar enhancements have been observed in radar backscattering of the newer craters by a number of workers (*1*). It has been hypothesized that in the creation of these craters dense material is uncovered or that the surface is compacted. Thus, relatively new features may be present at the locations given in Fig. 3.

The strength of the received signal may be used to estimate the signal levels which would be encountered in a planetary experiment in which the transmissions originate on Earth and are received on the spacecraft. The following set of radar parameters might be assumed: radiated signal power, 5×10^5 watts; antenna gain (transmitting), 65 db; antenna gain (receiving), 20 db; receiving-system noise temperature, 300–600°K. If these numbers are compared with the system characteristics of the experiment described here, the improvement in signal-to-noise ratios for the same range from transmitter to target and target to receiver is about 90 db, depending on the choice of system noise temperature. The scattering would still be 10 to 15 db stronger even if the target were located 1.0 A.U. away (on Venus, for example) and the orbiter were $1–2 \times 10^3$ km above the surface.

G. L. Tyler, V. R. Eshleman
G. Fjeldbo, H. T. Howard
A. M. Peterson

Center for Radar Astronomy,
Stanford University,
Stanford, California 94305

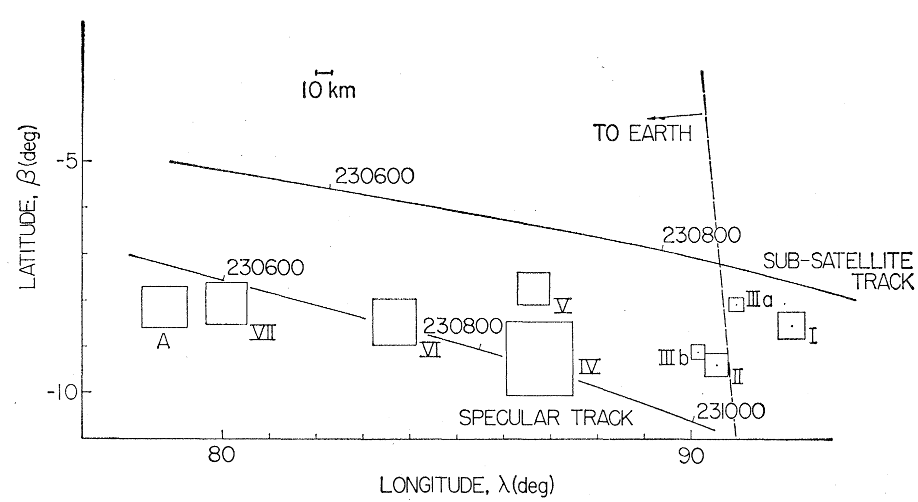

Fig. 3. Locations of scattering centers in selenographic latitudes and longitudes. The centers of the squares indicate location, while the size of the squares represents the estimate of the variance. In the case of the smaller values, the variance probably represents measurement error, but in the case of larger ones, such as IV, it is believed to be due to the extent of the target itself. The spacecraft ground track and the specular track are noted. The tick marks correspond to the positions along the track at the indicated times. The dashed line corresponds to the approximate limb of the moon at the time the data were taken. (A deviation of only a few hundred meters above the surface of the mean moon is required for an object at position I to be visible above the mean limb.)

References and Notes

1. G. H. Pettengill and J. C. Henry, *J. Geophys. Res.* **67**, 4881 (1962); T. W. Thompson and R. B. Dyce, *ibid.* **71**, 4861 (1966).
2. We thank the individuals at NASA headquarters, the Lunar Orbiter Project Office at Langley Research Center, and the Lunar Orbiter flight directors for their help. Supported by NASA under grant NSG-377.

30 March 1967